Materials Research Bulletin 95 (2017) 588–596

Contents lists available at ScienceDirect

Materials Research Bulletin

journal homepage: www.elsevier.com/locate/matresbu

Highly desirable semiconducting materials for mid-IR optoelectronics: Dilute bismide $InAs_{1-x}Bi_x$ alloys

Abdenacer Assali[a,b,*], M'hamed Bouslama[b], A.H. Reshak[c,d], Loubna Chaabane[e]

[a] Unité de Recherche en Optique et Photonique (UROP-Sétif) – Centre de Développement des Technologies Avancées, P.O. Box 17, Baba-Hassen, 16303 Algiers, Algeria
[b] Laboratoire Matériaux (LABMAT), Ecole Nationale Polytechnique d'Oran (ENPO), BP 1523 El Mnaouar, 31000 Oran, Algeria
[c] New Technologies – Research Centre, University of West Bohemia, Univerzitni 8, 306 14 Pilsen, Czech Republic
[d] School of Material Engineering, University Malaysia Perlis, 01007 Kangar, Perlis, Malaysia
[e] Laboratoire de Technologie des Matériaux et de Génie des Procèdes, Faculté de Technologie, Université A/MIRA-Bejaia, Route Targa-Ouzemour 06000, Algeria

ARTICLE INFO

Article history:
Received 17 February 2017
Received in revised form 7 May 2017
Accepted 8 June 2017
Available online 9 June 2017

Keywords:
$InAs_{1-x}Bi_x$ bismide alloy
mid-IR optoelectronics
FP-LAPW (TB-mBJ) method
Optoelectronic characteristics

ABSTRACT

We have performed a self-consistent full-potential linearized augmented plane wave (FP-LAPW) method within density functional theory (DFT) to investigate the structural, electronic and optical properties of the dilute bismide $InAs_{1-x}Bi_x$ alloys ($0 \le x \le 0.125$) for mid-IR optoelectronics application. The ground state properties including the lattice constant a_0 and bulk modulus B_0 are obtained by using Wu–Cohen generalized gradient approximation (WC-GGA), show agreement with experimental data. The calculated band gap energy (E_g) using Tran–Blaha-modified Becke–Johnson scheme (TB-mBJ) with spin-orbit coupling, show close agreement to experimental E_g. $InAs_{1-x}Bi_x$ alloys exhibits large band gap reduction for small Bi compositions (~380 meV for $x = 0.125$) covering the mid- and far-IR (~2.6–14 μm) wavelengths range. The narrow-band gap in $InAs_{1-x}Bi_x$ alloys can be attributed to the both resonant interaction of Bi-*p* states with the valence band maximum (VBM) and the hybridization (anticrossing) of the unoccupied *s*/*p* orbitals of In/As/Bi atoms with the host conduction band (CB). The dielectric functions and optical parametric quantities such as refractive index, extinction coefficient, absorption coefficient, reflectivity and energy loss function are determined for radiation range 0–10 eV in comparison with available experimental data. The critical-point (CP) energies have been identified from the computed electronic band structure in agreement with measured data. This makes $InAs_{1-x}Bi_x$ potential materials for fabrication advanced optoelectronic devices as photodetectors and laser diodes operating in the mid-IR wavelengths region.

© 2017 Elsevier Ltd. All rights reserved.

1. Introduction

In recent years, III–V-Bismides have attracted enormous interest for use in infrared (IR) optoelectronic applications for instance in fabrication laser diodes (LD's) and detectors [1–4]. Dilute bismide GaAsBi is particularly extremely important material, which currently applied in mid- and far-infrared optical [5] and spintronics [6] devices as well as multijunction solar cells [7]. The addition of dilute bismuth (Bi) amounts into GaAs results in a large reduction of band gap energy (*Eg*) (about 90 meV/% Bi) with a significant increase of the spin-orbit-splitting energy (Δ_{SO}) [8,9]. Similar band gap reduction is observed when introducing small contents of nitrogen (N) into GaAs (~200 meV/% N) [10]. There are also some characteristic differences between the dilute bismide GaAsBi and nitride GaAsN materials. The narrow band gap in GaAsBi alloys is due to the resonant interaction between the valence band maximum (VBM) and occupied Bi-*p* orbitals [11,12]. In the case of GaAsN, the nitrogen resonant *s* states interaction with the host conduction band [13,14] causes splitting of the conduction band (CB) due to the large size and electronegativity mismatch between N and As atoms [15,16]. Since GaAsBi materials have better optical and transport properties than nitride GaAsN alloys. This because the nitrogen incorporated (in GaAs) affect electronic structure by reducing electron mobility (≈300 $cm^2/V/s$) [17] and poor optical properties, allows to degrade the efficiency of optical

* Corresponding author at: Unité de Recherche en Optique et Photonique (UROP-Sétif) – Centre de Développement des Technologies Avancées, P.O. Box 17, Baba-Hassen, 16303 Algiers, Algeria.
E-mail address: assali_nacer@yahoo.fr (A. Assali).

http://dx.doi.org/10.1016/j.materresbull.2017.06.011
0025-5408/© 2017 Elsevier Ltd. All rights reserved.

devices. However, the effect of the Bi-induced on the electronic properties in particularly electron mobility is negligible [18].

GaAsBi crystals were successfully grown by Metal Organic Vapour Phase Epitaxy (MOVPE) [19] and Molecular Beam Epitaxy (MBE) [20]. Growth of narrow-gap bismide alloys likes InPBi [21] (by gas source MBE), InSbBi [22] (by MOVPE) and GaSbBi [23] (by MBE) have been investigated for long wavelength-infrared laser and detector applications.

Indium arsenide bismide is an important member of bismide family that exhibits small band gap energy, spans from (InAs) 0.42 eV [24] to (InBi) semimetal [25] with increasing Bi content. This makes InAsBi is very useful for develop of novel sources of light and photodetectors operating in the mid- and far-infrared (~3–30 μm) wavelengths range. The mid-IR wavelengths (~2–5 μm) optical devices are necessary for important applications such as optical gas sensor instrumentation, free-space optical telecommunications, laser surgery, thermal imaging and environmental monitoring [26]. Barnett et al. [27] were the first to predict InAsBi as a novel material system for mid-IR detectors in 1987. Since InAsBi system has been the subject of numerous review latters for both experimentally and theoretically. Experimentally, InAsBi with good quality layers was successfully grown by OMVPE for the first time by Ma et al. [28] in 1989. Fang et al. [29] used infrared photoluminescence (PL) to investigate InAsBi-grown by atmospheric pressure OMVPE at composition x rang up to 2.3%. Low-Pressure MOVPE growth of metastable InAsBi has been latter demonstrated (in 1998) by Okamoto and Oe [30]. Recently, Svensson et al. [31] reported photoluminescence properties of InAsBi-grown by MBE. Sandal et al. [32] realized InAsBi photodiode by MBE-STM technique. They found spectral response from the diode up to a diode temperature of 225 K and Bi-incorporated reduce the band gap of InAs by 75 meV. Quite recently, the investigation of MBE-grown InAsBi (x ~4.5% and ~5.8%) films by transmission electron microscopy was reported by Lu et al. [33]. On the theoretical side, Polak et al. [34] calculated Bi-induced changes in the band structure of In–V–Bi (InAsBi) alloys with Bi ≤ 3.7% within the DFT theory as implemented in ABINIT code. Samajdar et al. [35] presented an investigation of the valence band structures of InAsBi, InSbBi and InPBi using the Valence band anticrossing (VBAC) model. Quantum dielectric Theory (QDT) was used to deduce the band gap bowing effect in III–V-Bi alloys by Samajdar and Dhar [36].

Due to their smaller band gap, high electron mobility (20.000 $cm^2 V^{-1} s^{-1}$) and relative thermal stability (melting point of 942 °C) [37], InAs is applied for a wide range of applications involving speed and electro-optical devices [38,39]. At ambient conditions, InAs crystallize in the cubic zinc-blende structure (space group $F43m$) with a lattice parameter equal to 6.058 Å at room temperature [40].

In the present paper, we use self-consistent FP-LAPW method based on DFT theory for calculating the structural, electronic and optical properties of zinc blende $InAs_{1-x}Bi_x$ alloys over the composition x range $0 \le x \le 0.125$, and the results were compared to experimental data. We found $InAs_{1-x}Bi_x$ system with useful properties for mid-IR optoelectronics application.

2. Method of calculations

The first-principles calculations are performed by employing a full-potential linearized augmented plane wave (FP-LAPW) method within density functional theory (DFT) [41,42] as implemented in the WIEN2K package [43]. The exchange-correlation potential for the structural properties was treated by the new form of generalized gradient approximation (WC-GGA) established by Wu and Cohen [44], which is efficient for geometry optimization. We used the powerful scheme modified Becke–Johnson (TB-mBJ) [45] for predicting the electronic structure. The spin-orbit coupling (SOC) is included in the calculation of the band gaps and DOS of these alloys. The optical properties were determined by TB-mBJ scheme.

It is well known that the standard approaches such as GGA and LDA are insufficient for electronic structure calculations, it usually underestimate the band gap of semiconductor and insulator materials by about 30–50% than the experimental values [46–48]. However, the modified Becke-Johnson exchange potential + *GW* methods [49]. It is a semilocal approximation to an atomic "exact-exchange" potential and a screening term. This is just a XC-potential, not a XC-energy functional, thus Exc is taken from LSDA (GGA) and the forces cannot be used with this option.

The wave functions, charge density and potential inside the muffin-tin (MT) spheres are expanded with an angular momentum equal to $l_{max} = 10$. In order to achieve energy convergence, we have expanded the basis function up to $R_{MT}K_{max} = 7$ (R_{MT} is the average radius of the spheres muffin-tin and K_{max} is the maximum value of the vector Wave K). We have chosen the muffin-tin radii R_{MT} to be about 2.4, 2.25 and 2.6 a.u. for In, As and Bi, respectively. The In ($4d^{10}\,5s^2\,5p^1$), As ($4d^{10}\,5s^2\,5p^1$) and Bi ($4f^{14}\,5d^{10}\,6s^2\,6p^3$) states are treated as valence electrons. A Monkhorst – Pack mesh [50] of 47 special k-points (grid of $10 \times 10 \times 10$) was used for the binary InAs and 20 special k-points (grid of $7 \times 7 \times 7$) for ternary alloys $InAs_{1-x}Bi_x$ in the irreducible wedge of the Brillouin zone (IBZ).

In order to model $InAs_{1-x}Bi_x$ alloys at compositions $x = 0$, 0.031, 0.062, 0.093 and 0.125, we applied a 64-atom supercell $In_{32}As_{32-n}Bi_n$ which corresponds to $2 \times 2 \times 2$ conventional zinc blend cell. All considered structures were crystallizes in the zinc blend structure, $InAs_{1-x}Bi_x$ structures were relaxed by minimizing the forces exerted on the atoms to displace it into the equilibrium positions within self-consistent FP-LAPW calculations. Fig. 1 displays the zinc blend structure for $InAs_{1-x}Bi_x$ at $x = 0.031$ and 0.093.

3. Results and discussion

3.1. Structural properties

The ground state properties of zinc-blende ternary $InAs_{1-x}Bi_x$ alloys for compositions $x = 0$, 0.031, 0.062, 0.093 and 0.125 are determined by the total energy calculations based on FP-LAPW method within WC-GGA approximation. The total energies are calculated as a function of volume and fitted to Murnaghan equation of state [51]. The results of the equilibrium lattice constants a_0, bulk modulus B_0 and its derivative of these compounds are listed in Table 1 along with experimental and previous theoretical values. The lattice constant of InAs is obtained to be 6.092 Å, which is very close to experimental data of 6.058 Å [52] and the theoretical value of 6.091 Å calculated by DFT within WC-GGA approach [53] which is better than those results obtained by GGA (6.20 Å) and LDA (5.956 Å). The predicted bulk modulus B_0 of 57.17 GPa for InAs is very consistent to experimental data of 58 GPa [56] and other WC-GGA value of 54.99 GPa [53].

The dependence composition of the lattice constant a_0 on the Bi content x for zinc blende $InAs_{1-x}Bi_x$ alloys is given as

$$a_{InAs_{1-x}Bi_x} = x a_{InBi} + (1-x) a_{InAs} - x(1-x) b \quad (1)$$

where b represents the bowing parameter, a_{InBi} and a_{InAs} are the lattice constants of InBi and InAs, respectively.

The calculated lattice constant a_0 of zinc blende $InAs_{1-x}Bi_x$ alloys as a function of Bi content x is depicted in Fig. 2 and compared to the linear Vegard's law [57]. The lattice constant deceases almost linearly with increasing small amounts of Bi (up to 0.125) over a range of 8.4%. The best fit results with Eq. (1), the

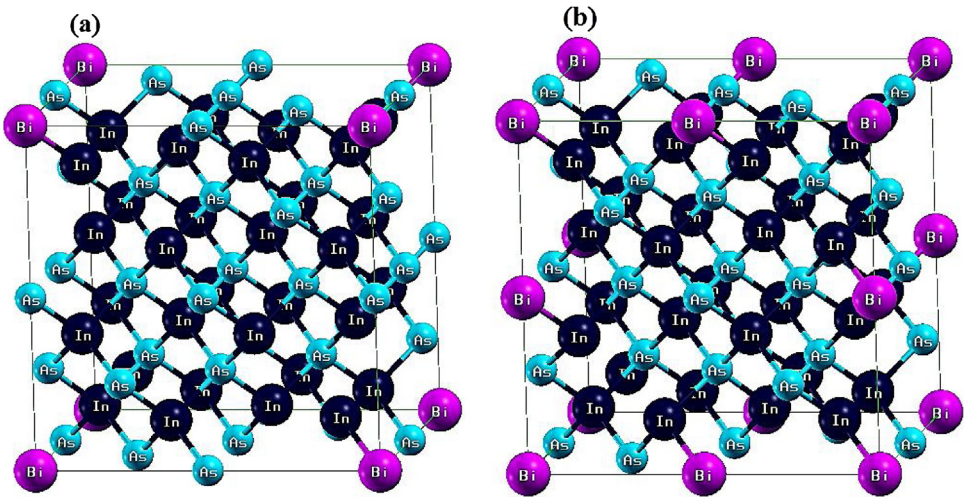

Fig. 1. Zinc blende structure of $InAs_{0.968}Bi_{0.031}$ (a) and $InAs_{0.906}Bi_{0.093}$ (b) (64-atom supercells 2a × 2b × 2c).

Table 1
Calculated lattice constant *a* (Å), bulk modulus *B* (GPa) and derivative of bulk modulus *B'* for $InAs_{1-x}Bi_x$ alloys ($0 \le x \le 0.125$) compared with experimental and previous theoretical values.

	Lattice constant (Å)			Bulk modulus (GPa)			*B'*	
Components	WC-GGA	Expt.	Theory	WC-GGA	Expt.	Theory	WC-GGA	Refs.
InAs	6.092	6.058[a]	6.091[b]–6.20[c]–5.956[d]	57.17	58[e]	54.99[b] –49.1[c] –65.7[d]	4.27	[a]Ref. [5]
$InAs_{0.968}Bi_{0.031}$	6.116			55.84			4.95	[b]Ref. [53]
$InAs_{0.937}Bi_{0.062}$	6.137			54.85			5.14	[c]Ref. [54]
$InAs_{0.906}Bi_{0.093}$	6.157			54.08			5.19	[d]Ref. [55]
$InAs_{0.875}Bi_{0.125}$	6.176			53.62			5.10	[e]Ref. [56]

lattice constant $a(x)$ for ZB $InAs_{1-x}Bi_x$ can be expressed as

$$a_{InAs_{1-x}Bi_x} = 6.09243 + 0.68425x - 0.08777x^2 \quad (2)$$

The quasi linear behavior of lattice constant *a* (from Vegard's law) is observed with an downward bowing of 0.08777 Å for contents $x \le 0.125$ which agree well with the experiments of Ma et al. [58] and Huang et al. [59] with $x \le 0.04$. This behavior has been also observed for bismides $InSb_{1-x}Bi_x$ [60] and $GaAs_{1-x}Bi_x$ [61] as well as other III-nitrides such as $Ga_xAs_{1-x}N$ [62], $Tl_xAl_{1-x}N$ [63] and $Tl_xGa_{1-x}N$ [64]. The bowing parameter is obtained marginal less than 0.00769 Å for higher Bi composition *x* up to 1, as shown in the inset of Fig. 2. The bowing parameter is a consequence of the relaxation effect of In–Bi and As–Bi bond lengths and the lattice mismatch between the parent binaries InAs and InBi. It should be noted also that the structural relaxation considerably reduce the bowing parameter leading to a linear behavior of the lattice constants a_0 with composition *x* [65,66]. Fig. 3 shows the calculated bulk modulus B_0 of zinc blende $InAs_{1-x}Bi_x$ alloys as a function of Bi content *x* and compared to the linear concentration dependence (LCD). It is found that the bulk modulus decreases by the increase of Bi content *x*. A significant deviation of the bulk modulus from the LCD is observed due to the

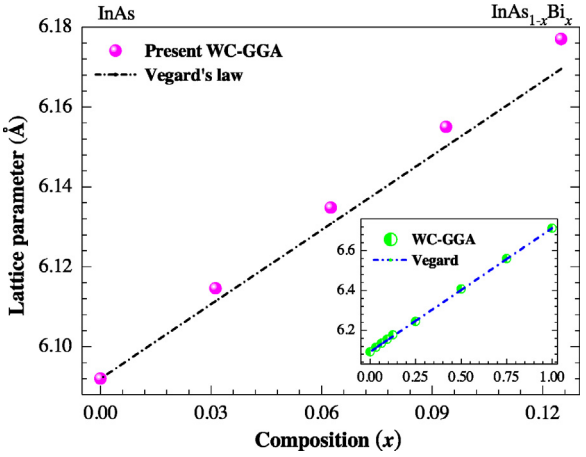

Fig. 2. Lattice parameter of zinc blende $InAs_{1-x}Bi_x$ as a function of bismuth content *x*. The inset shows the dependence composition of $a(x)$ with $0 \le x \le 1$.

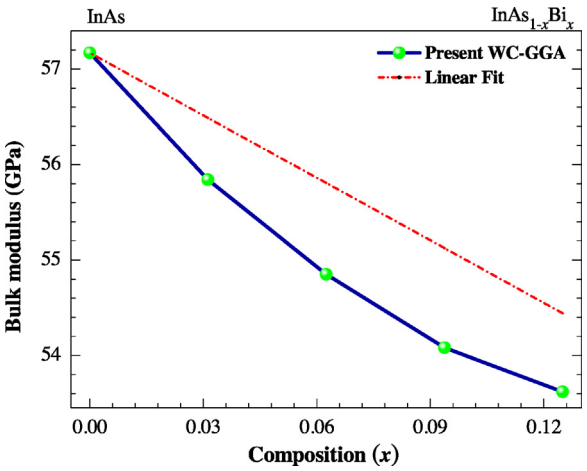

Fig. 3. Bulk modulus of zinc blende $InAs_{1-x}Bi_x$ as a function of bismuth content *x*.

large mismatch between the bulk modulus of the binary InAs and InBi compounds. This suggests that $InAs_{1-x}Bi_x$ becomes more compressible by increasing Bi content.

3.2. Electronic properties

3.2.1. Band structure

Electronic band structure of zinc blende $InAs_{1-x}Bi_x$ ($0 \leq x \leq 0.125$) based on self-consistent scalar relativistic FP-LAPW plus spin-orbit coupling (SOC) calculations within TB-mBJ exchange potential are investigated in this section. The calculated energy gaps are listed in Table 2 along with previous DFT calculations and the experimental data. The gap energy for InAs compound is found to be 0.60 eV (without SOC) and 0.467 eV (with SOC) in excellent agreement with the experimental data of (0.417 [67], 0.42 [68]) and other TB-mBJ values of (0.615 eV [53], 0.593 eV [69]) (without SOC). Our results are close to experimental data compared to those obtained from the standard GGA (−0.61 eV [54], 0.00 eV [70]) and LDA (0.00 eV [71]) approximations. Since TB-mBJ shows better overall agreement with the experimental data, the TB-mBJ band structure for zinc blende $InAs_{0.968}Bi_{0.031}$ and $InAs_{0.906}Bi_{0.093}$ are plotted in Fig. 4 along the high symmetry points. It is clearly seen that the maximum of the valence band (VBM) and the minimum of the conduction band (CBM) are located at the Γ symmetry point of the Brillouin zone. Consequently, the zinc blende $InAs_{1-x}Bi_x$ alloys exhibit direct-band gaps, which is very useful for optical transitions.

The dependence of band gap (E_g) on the Bi content x is given by the flowing relation

$$E_g = xE_{InBi} + (1-x)E_{InAs} - x(1-x)b \quad (3)$$

where b is the optical bowing parameter, E_{InBi} and E_{InAs} are the gap energies of InBi and InAs, respectively.

Fig. 5 shows the calculated band gap energy of zinc blende $InAs_{1-x}Bi_x$ alloys as a function of Bi content x using TB-mBJ functional in comparison to the available experimental data. It has been found that the energy gap of $InAs_{1-x}Bi_x$ alloys decreases by around 380 meV when small amount of Bi is added. For instance, the energy gap decreases from 0.467 eV ($x = 0$) to 0.087 eV ($x = 0.125$), covering the optical wavelengths of ~2.6–14 μm in the middle and far infrared region. Which is of great interest for designing QW lasers and detectors operating in the mid- and far-IR spectrum region.

The obtained results were fitted by using the Eq. (3), the analytical expression of band gap for $InAs_{1-x}Bi_x$ as a function of composition x is given as

$$E_g^{TB-mBJ} = 0.46414 - 2.94029x - 0.58368x^2 \quad (4)$$

The gap energy varies non-linearly with composition x where exhibits a small optical band gap bowing parameter equal to 0.58368 eV. This gap bowing value is larger than that determined by Polak et al. [34] of about 4.2 eV with $x \leq 0.037$ calculated using the valence band anticrossing (VBAC) model. The reason for this discrepancy might be due to the dependence of bowing parameter

Table 2
Energy gaps for $InAs_{1-x}Bi_x$ alloys ($0 \leq x \leq 0.125$) compared with experimental data and other theoretical works.

	Energy gap (eV)			
Components	TB-mBJ	Expt.	Theory	Refs.
InAs	0.467	0.417[a] – 0.42[b]	0.593[c]–0.615[d]–0.61[e]–0.00[f]– 0.00[g]	[a]Ref. [67] [b]Ref. [68] [c]Ref. [69] [d]Ref. [53] [e]Ref. [54] [f]Ref. [70] [g]Ref. [71]
$InAs_{0.968}Bi_{0.031}$	0.362			
$InAs_{0.937}Bi_{0.062}$	0.287			
$InAs_{0.906}Bi_{0.093}$	0.180			
$InAs_{0.875}Bi_{0.125}$	0.087			

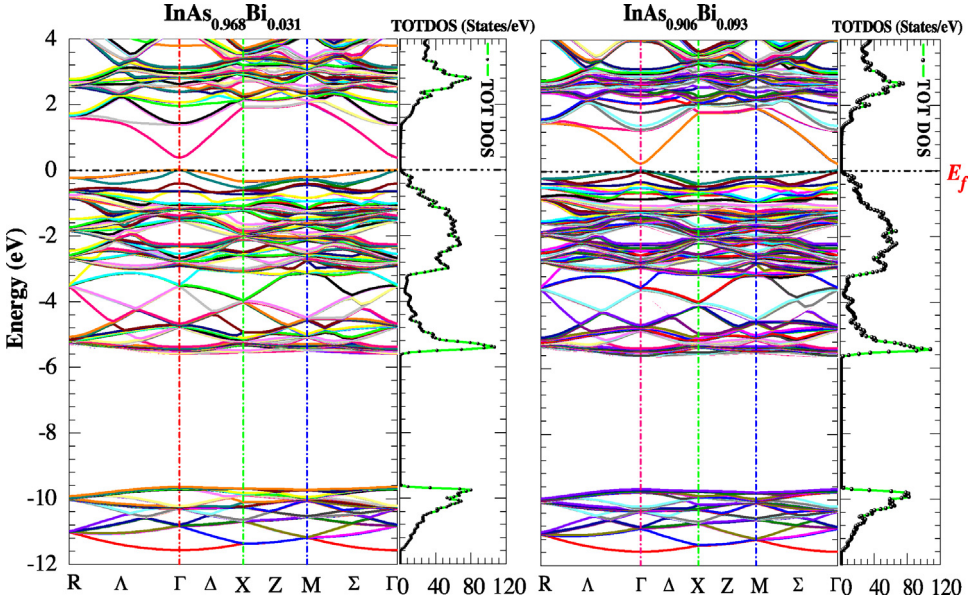

Fig. 4. Band structure and total TDOS for zinc blende $InAs_{0.968}Bi_{0.031}$ and $InAs_{0.906}Bi_{0.093}$ obtained from TB-mBJ potential. The Fermi level (E_f) is set to energy zero.

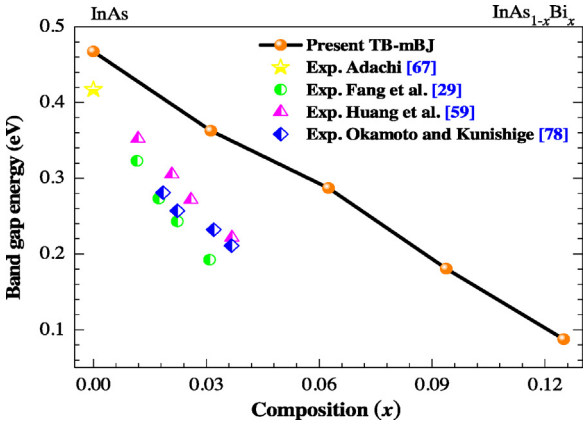

Fig. 5. Band gap energies of zinc blende $InAs_{1-x}Bi_x$ as a function of bismuth content x obtained from TB-mBJ potential and compared to experimental data.

on content x which decreases with increasing x [72,73], and of course to the method of calculation. The origin of band gap bowing is due to the atomic size difference and electronegativity mismatch between Bi and As atoms in $InAs_{1-x}Bi_x$ alloys. It has been found that a significant bowing at small content x is not due to the mismatch between the parent binaries but it is a consequence to the resonant wave function inside the valence band [73,74]. However, our value of b is quite similar to those obtained for other III–V semiconductor alloys such as $InAs_{1-x}Sb_x$ (0.58 eV [75]), $InGa_{1-x}As_x$ (0.40 eV [76]) and $InGa_{1-x}P_x$ (0.45 eV [77]). Furthermore, the Bi-induced band gap reduction in $InAs_{1-x}Bi_x$ is in reasonable agreement with experimental data reported by Fang et al. [29], Huang et al. [59] and Okamoto and Oe [78].

3.2.2. Density of states

In order to analyze the origin of the electronic band structure of these alloys, the total (TDOS) and partial (PDOS) densities of states for $InAs_{1-x}Bi_x$ alloys are calculated using TB-mBJ potential with SOC for energy range −12–8 eV. The TDOS and PDOS for ZB $InAs_{0.968}Bi_{0.031}$ and $InAs_{0.906}Bi_{0.093}$ are plotted in Fig. 6(a,b), as prototypes. We observed that these curves are similar for both

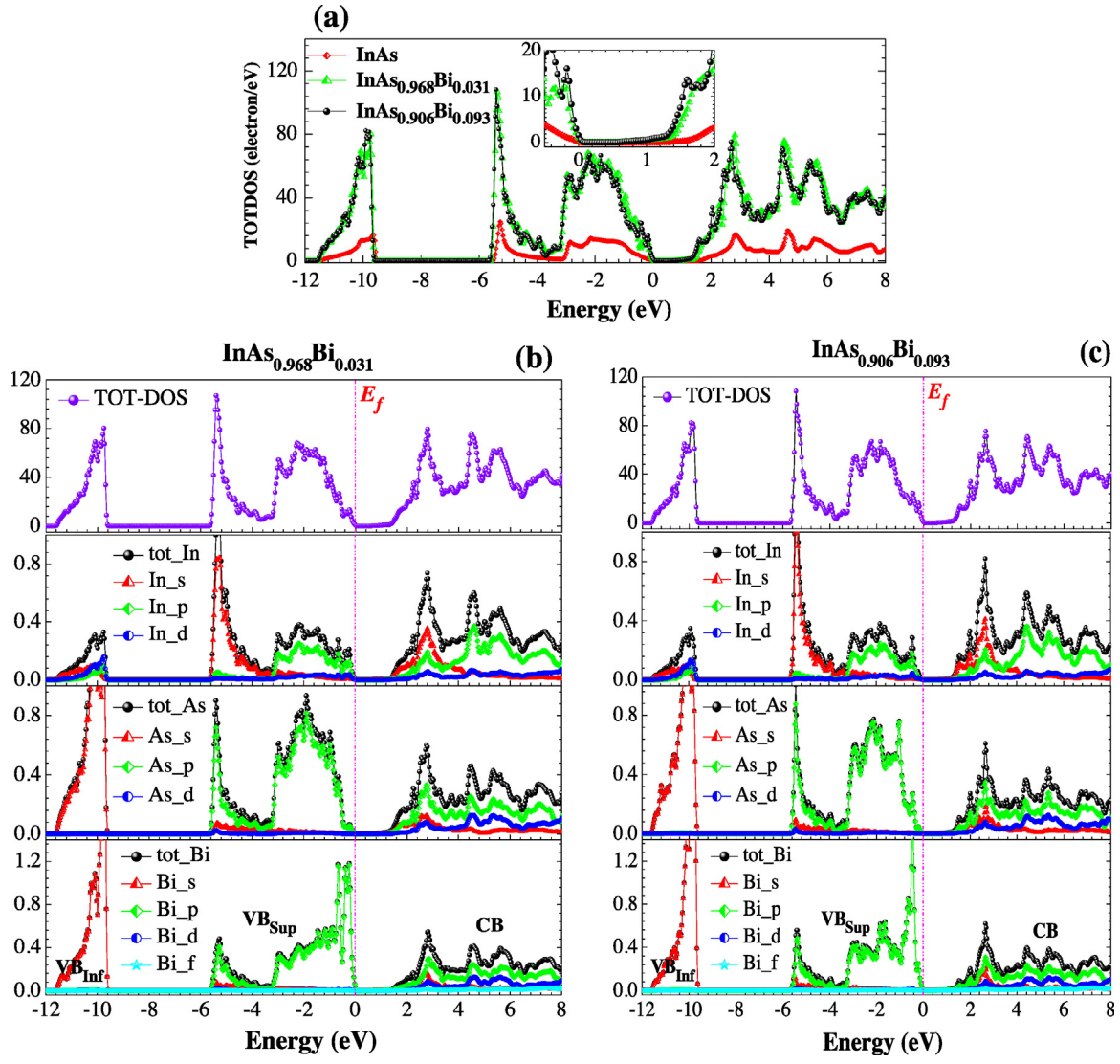

Fig. 6. Total (TDOS) and partial (PDOS) densities of states for zinc blende $InAs_{0.968}Bi_{0.031}$ and $InAs_{0.906}Bi_{0.093}$ obtained from TB-mBJ potential.

alloys. According to Fig. 6(a,b), we can distinguish, from the top of the valence band, two regions separated by gaps called (VB_{Inf}, VB_{Sup}) and a region of conduction band CB. The inferior energy group VB_{Inf} from −11.6 eV to −9.6 eV is mainly due to the contribution of the orbitals *s* of As/Bi atoms. The superior group VB_{Sup} below the Fermi level (E_f) is divided into two regions different. The first one occurs between −5.7 eV and −3.2 eV is dominated by In-*s* and As-*p* orbitals with a small contribution of Bi-*p* state. The region localized in the top of the valence band range from −3.2 eV to 0.0 eV consists by participation of In/As/Bi-*p* orbitals. The conduction band CB is formed by hybridization between In-*s*/*p*, As-*p* and Bi-*p* states.

To understand the origin of the Bi-induced changes in band gap of $InAs_{1-x}Bi_x$, we plot in Fig. 6(a) the TDOS at different concentrations $x = 0$, 0.031 and 0.093. As seen in Fig. 6(a), the valence band shifts to towards the Fermi level with the increase of the Bi content, while the conduction band is small downward tends to reduce the band gap. It is shown that VBM is mainly contributed by B-*p* state and the CBM is formed by hybridization between the unoccupied In-*s* and As/Bi-*p* orbitals. Thus, the reduction in band gap is due to both a band-anticrossing interaction between the VBM and localized Bi-*p* resonant states and the hybridization (anticrossing) between In-*s*/*p*, As-*p* and Bi-*p* states with the CBM. The Bi-induced changes in the VB and CB have also been observed for similar bismides $InSb_{1-x}Bi_x$ [60] and $InP_{1-x}Bi_x$ [34].

3.3. Optical properties

The knowledge of optical parametric quantities is essentially for better understanding the materials properties for their applications in optical device design. The optical parameters for zinc blende $InAs_{1-x}Bi_x$ alloys at different compositions *x* (0, 0.031, 0.062, 0.093 and 0.125) are presented in this part using the accurate scheme TB-mBJ. All optical functions can be described from the complex dielectric function $\varepsilon(\omega)$ given as

$$\varepsilon(\omega) = \varepsilon_1(\omega) + i\varepsilon_2(\omega) \quad (5)$$

where $\varepsilon_1(\omega)$ and $\varepsilon_2(\omega)$ are the real and imaginary parts of the dielectric function, respectively. $\varepsilon(\omega)$ is known to describe the optical response of the medium at photon energies $E = \hbar\omega$ [79]. The imaginary part $\varepsilon_2(\omega)$ of the dielectric function is calculated by the joint density of states, $J_{cv}(E)$, between the conduction band (CB) and the valence band (VB). The real $\varepsilon_1(\omega)$ can be extracted from the imaginary $\varepsilon_2(\omega)$ part using the Kramers–Kroning relationship [80,81], using the expressions:

$$\varepsilon_1(\omega) = 1 + \frac{2}{\pi} P \int_0^{\infty} \frac{\omega' \varepsilon_2(\omega')}{(\omega'^2 - \omega^2)} d\omega' \quad (6)$$

$$\varepsilon_2(\omega) = \left(\frac{4\pi^2 e^2}{m^2\omega^2}\right) \sum_{ij} \int |\langle i|M|j\rangle|^2 f_i(1 - f_j) \times \delta(E_f - E_i - \omega) d^3k \quad (7)$$

where *M* is the dipole matrix, *i* and *j* are the initial and final states respectively, f_i is the Fermi distribution for the *i*th state.

The optical constants include refractive index $n(\omega)$, extinction coefficient $k(\omega)$, absorption $\alpha(\omega)$, reflectivity $R(\omega)$ and energy loss function $L(\omega)$ are derived from the complex dielectric function $\varepsilon(\omega)$ [82,83]:

$$n(\omega) = \frac{1}{\sqrt{2}\left[\sqrt{\varepsilon_1^2(\omega) + \varepsilon_2^2(\omega)} + \varepsilon_1(\omega)\right]^{1/2}} \quad (8)$$

$$k(\omega) = \frac{1}{\sqrt{2}\left[\sqrt{\varepsilon_1^2(\omega) + \varepsilon_2^2(\omega)} - \varepsilon_1(\omega)\right]^{1/2}} \quad (9)$$

$$\alpha(\omega) = \sqrt{2}(\omega)\left[\sqrt{\varepsilon_1^2(\omega) + \varepsilon_2^2(\omega)} - \varepsilon_1(\omega)\right]^{1/2} \quad (10)$$

$$R(\omega) = \left[\frac{\sqrt{\varepsilon_1^2(\omega) + j\varepsilon_2^2(\omega)} - 1}{\sqrt{\varepsilon_1^2(\omega) + j\varepsilon_2^2(\omega)} + 1}\right]^2 \quad (11)\; L(\omega) = \mathrm{Im}\left(\frac{-1}{\varepsilon(\omega)}\right) = \left[\frac{\varepsilon_2(\omega)}{\varepsilon_1^2(\omega) + \varepsilon_2^2(\omega)}\right] \quad (12)$$

The real $\varepsilon_1(\omega)$ and imaginary $\varepsilon_2(\omega)$ parts of the dielectric function for $InAs_{1-x}Bi_x$ alloys calculated from TB-mBJ functional in the photon energy range 0–10 eV are displayed in Fig. 7 in comparison to available measured data. The imaginary part is an important factor which related to the optical electronic transitions raised in materials. As shown in Fig. 7(b), the absorption edge in ε_2 occurs at about 0.58, 0.56, 0.52, 0.49 and 0.47 eV for composition $x = 0$, 0.031, 0.062, 0.093 and 0.125, respectively. This corresponds to direct optical transition from the highest valence to the lowest conduction bands at Γ point (Γ_{15v}–Γ_{1c}). For InAs, ε_2 shows strongest peaks E_1 and E_2 at energies ~2.6 and ~4.47 eV due to the interband transitions at symmetry points L_{3v}–L_{1c} and X_{5v}–X_{1c},

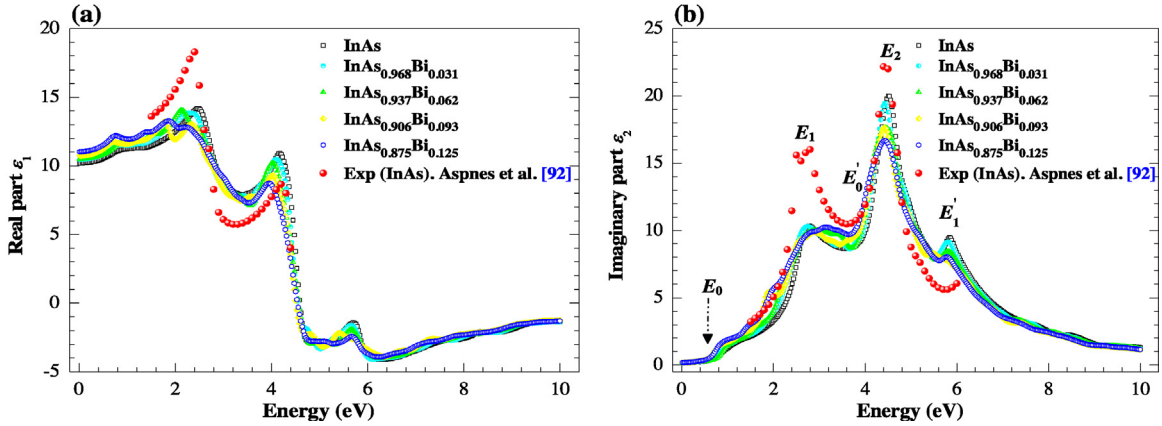

Fig. 7. Real $\varepsilon_1(\omega)$ (a) and imaginary $\varepsilon_2(\omega)$ (b) parts for $InAs_{1-x}Bi_x$ alloys obtained from TB-mBJ potential. The measured data for InAs is taken from [92].

respectively. The E'_0 peak arises at ~3.9 eV is mainly corresponds to the transition Γ_{15v}–Γ_{15c}. The latest peak E'_1 is located at around 5.8 eV related to the L_{3v}–L_{3c} transition. In $InAs_{1-x}Bi_x$, the contributions of the critical-points (CPs) in ε_2 are due to the direct transitions between the occupied In/As/Bi-*p* states localized at the VBmaximum to unoccupied In-*s*/*p*, P-*p* and Bi-*p* orbitals localized in the CBminimum along *R*,Γ and *X* direction in the Brillouin Zone, as shown in Figs. 5 and 6. The critical-point (CP) energies are summarized in Table 3. It can be seen that the present CP energies for InAs are much closer to measured ellipsometric data. Also, the value of E_2 peak in ε_2 is 20.15 at 4.47 eV in well agreement with experimental values obtained by Aspnes and Studna of 22.8 at 4.44 eV [85], 22.61 at 4.45 eV [92] and Philipp and Ehrenreich of 21 [93]. We observe that all ε_2 structures are shifted towards lower energies due to the decreases in the optical band gap when increasing *x*. The peaks intensity decreases with content *x*, for E_2 transitions from 20.15 ($x = 0$) to 16.84 ($x = 0.125$). As seen in Fig. 7(a), ε_1 reaches maximum values at energies ~2.45 and ~4.2 eV related to E_1 and E_2 transitions afterwards full down at higher energies. Beyond ~4.5 eV, ε_1 becomes negative. In this energy range, occurring the reflectiveness of materials for the incident electromagnetic waves [94], and $InAs_{1-x}Bi_x$ alloys exhibit a

Table 3
Critical-point (CP) energies (in eV) in ε_2, static dielectric constant $\varepsilon_1(0)$ and static refractive index $n(0)$ for $InAs_{1-x}Bi_x$ alloys compared with available experimental and other theoretical data.

Components	Critical-points (CPs)							
	E_0	E_1	E'_0	E_2	E'_1	$\varepsilon_1(0)$	$n(0)$	Refs.
InAs	0.58; 0.45[a] 0.36[c] 0.36[e]	2.60; 2.57[a] 2.48[d] 2.50[e]	3.90; 3.90[a]	4.47; 4.44[b] 4.39[d] 4.45[e]	5.80; 6.40[a] 6.14[d]	10.18; 14.30[f] 15.15[h] 09.94[j]	3.19; 3.50[g] 3.60[i] 3.21[c]	[a]Ref. [84] [b]Ref. [85] [c]Ref. [86] [d]Ref. [87]
$InAs_{0.968}Bi_{0.031}$	0.56	2.57	3.86	4.43	5.78	10.31	3.21	[e]Ref. [88] [f]Ref. [67]
$InAs_{0.937}Bi_{0.062}$	0.52	2.55	3.82	4.41	5.76	10.47	3.23	[g]Ref. [89] [h]Ref. [90]
$InAs_{0.906}Bi_{0.093}$	0.49	2.51	3.79	4.38	5.74	10.75	3.27	[i]Ref. [91] [j]Ref. [69]
$InAs_{0.875}Bi_{0.125}$	0.47	2.50	3.77	4.34	5.76	11.02	3.32	

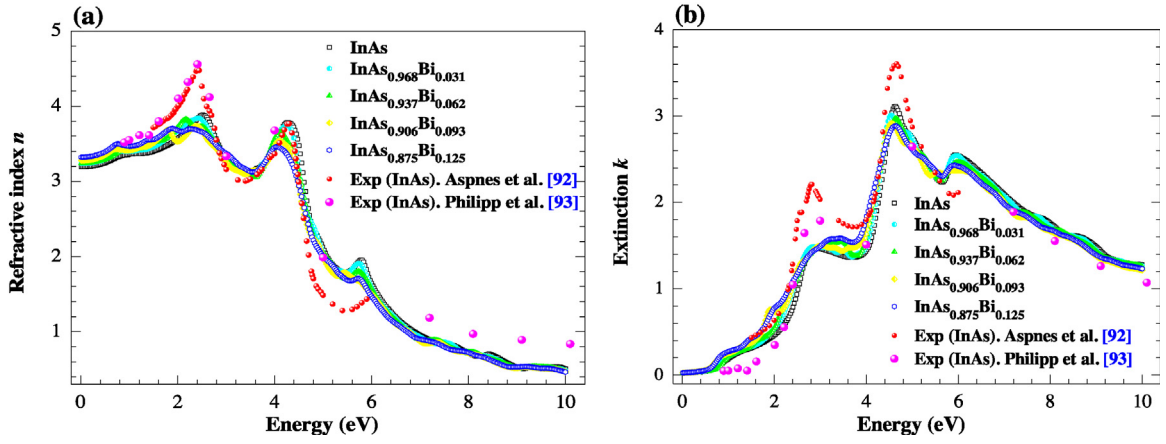

Fig. 8. Refractive index n(w) (a) and extinction coefficient k(ω) (b) for InAs1−xBix alloys obtained from TB-mBJ potential. The measured data for InAs is taken from [92,93].

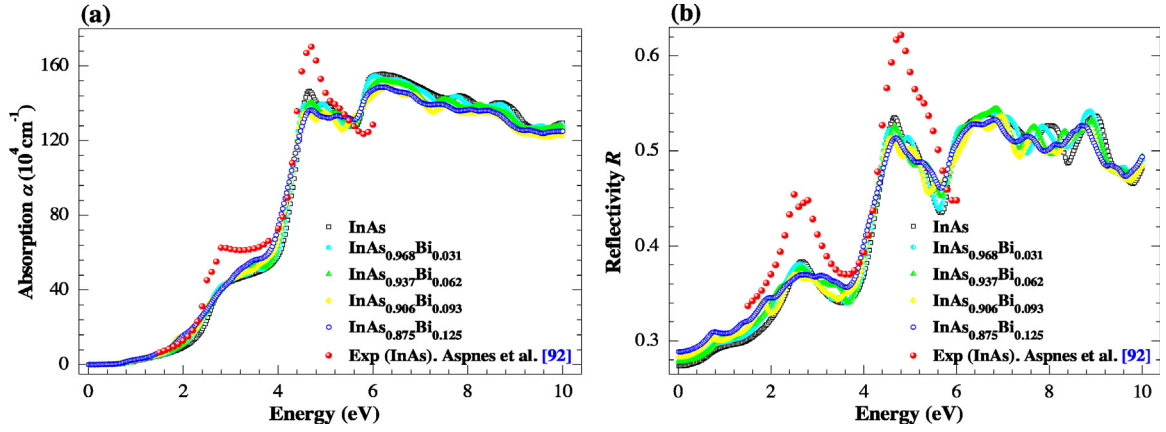

Fig. 9. Absorption coefficient α(ω) (a) and reflectivity $R(\omega)$ (b) for $InAs_{1-x}Bi_x$ alloys obtained from TB-mBJ potential. The measured data for InAs is taken from [92].

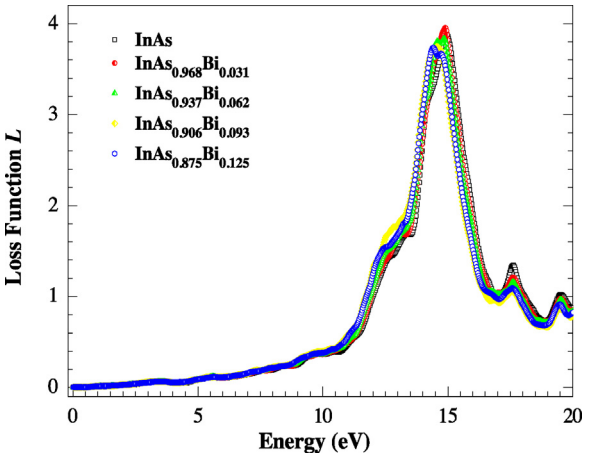

Fig. 10. Energy loss function $L(\omega)$ for $InAs_{1-x}Bi_x$ alloys obtained from TB-mBJ potential.

metallic character. The overall features of the calculated ε_1 and ε_2 are in reasonable good agreement with experiment [92]. The calculated static dielectric constant $\varepsilon_1(0)$ are listed in Table 3. Our results are comparable with experimental and other theoretical data. It has been noticed that the static $\varepsilon_1(0)$ decreases with the increase of content x.

Fig. 8 represents the calculated refractive index $n(\omega)$ and extinction coefficient $k(\omega)$ for $InAs_{1-x}Bi_x$ alloys. In Fig. 8(a), the refractive index n spectra exhibits maxima at energies about 2.6 and 4.3 eV due to the transitions E_1 and E_2, respectively. The static refractive index $n(0)$ values are given in Table 3 in good agreement with other experimental and theoretical data. The static n increases with increasing x. As seen in Fig. 8(b), the extinction k curves firstly increases to maximum value at ~4.65 eV then drops sharply at the highest energies. Our calculated n and k spectra agree very well with experiments [92,93].

The absorption coefficient $\alpha(\omega)$ and normal-incidence reflectivity $R(\omega)$ curves for $InAs_{1-x}Bi_x$ alloys are showed in Fig. 9. The absorption α has a zero value below the absorption edge (~0.58, 0.56, 0.52, 0.49 and 0.47 eV) (IR region) for each composition x. Beyond these points, α curves increases rapidly to achieve the highest values at the range of about 4.6–10 eV in the Ultraviolet (UV) region. The strongest peak occurs at 4.7 eV is corresponds mainly to E_2 transitions. The peak-energy E_1 is appears at lower photon energy around 2.6 eV. The reflectivity R in Fig. 9(b) show maximum value around 0.54 at the range ~4.6–10 eV ascribed to the resonance plasmon in the UV region. In R spectrum of InAs distinct two main peaks occur at ~2.52 and ~4.7 eV. These peaks result from the transitions E_1 and E_2 agrees reasonably well with the measured data of 2.53 (E_1) and 4.72 (E_2) [92]. The present α and R curves are quite good agreement with experiment [92]. All optical structures in n, k, α and R are shifted towards the lower energies with reduces of their peak heights when the Bi amounts increases.

In Fig. 10 we display the energy loss function $L(\omega)$ for $InAs_{1-x}Bi_x$ alloys in the photon energy range 0–20 eV. The plasmon losses are due to collective excitations of the valence electrons and their energies are corresponding to the density of valence electrons. For inter-band transitions, which consist mostly of plasmon excitations, the scattering probability for volume losses is directly connected to the energy loss function [95]. It can be seen that no energy loss produced in the range about 0–10 eV, this because of the imaginary part ε_2 is strong at these energies. The energy loss function has a maximum at a plasma resonance in the 14–15 eV photon energy range, where ε_2 is lower. Two smallest plasmon peaks occur at highest energies ~17.6 and ~19.5 eV.

4. Conclusion

We have investigated the structural, electronic and optical properties of the dilute bismide $InAs_{1-x}Bi_x$ alloys by employed the FP-LAPW method within DFT theory. The calculated structural parameters (a_0, B_0) using WC-GGA show agreement with the available experimental data and the theoretical results. Our calculated energy band gaps using TB-mBJ potential found to be in reasonable agreement with experimental band gaps. Bismuth substitution in $InAs_{1-x}Bi_x$ causes a band gap reduction of about 380 meV for $x = 0.125$ covering the optical wavelengths range of ~2.6–14 μm in the mid- and far-IR spectrum region. This reduction in band gap is a consequence to a band-anticrossing interaction between the host conduction band and higher-lying localized Bi-p resonant states. The dielectric functions and optical constants such as the refractive index $n(\omega)$, extinction coefficient $k(\omega)$, absorption $\alpha(\omega)$, reflectivity $R(\omega)$ and energy loss function $L(\omega)$ of these alloys are determined and the results are in satisfactory agreement with the available experimental data. The interband contributions to the optical functions are analyzed along with the computed electronic band structure. We find that the main peaks resolved in optical spectra result from the transitions E_1, E'_0, E_2 and E'_1 and the CPs agrees well with the measured data. All optical structures in n, k, α, R, L are shifted towards lower energies with peak heights reduction when the Bi content increases. As a result, $InAs_{1-x}Bi_x$ alloys are very useful for use in the production of highly efficient photodetectors and novel light sources as; laser diodes and LEDs suitable for emission in the mid-IR spectral region.

Acknowledgments

A. Assali would like to thank Pr. K. Bouamama (Université Ferhat Abbas Sétif 1) as well for his precious help. For A. H. Reshak, the result was developed within the CENTEM project, reg. no. CZ.1.05/2.1.00/03.0088, co-funded by the ERDF as part of the Ministry of Education, Youth and Sports OP RDI program and, in the follow-up sustainability stage, supported through CENTEM PLUS (LO1402) by financial means from the Ministry of Education, Youth and Sports under the "National Sustainability Program I. Computational resources were provided by MetaCentrum (LM2010005) and CERIT-SC (CZ.1.05/3.2.00/08.0144) infrastructures.

References

[1] T. Tiedje, E.C. Young, A. Mascarenhas, Int. J. Nanotechnol. 5 (2008) 963–983.
[2] Y. Zhang, A. Mascarenhas, L.-W. Wang, Phys. Rev. B 71 (2005) 155201.
[3] N. Hossain, I.P. Marko, S.R. Jin, K. Hild, S.J. Sweeney, R.B. Lewis, D.A. Beaton, T. Tiedje, Appl. Phys. Lett. 100 (2012) 051105.
[4] S.A. Khan, S. Azam, O. Sipr, Mater. Sci. Semicond. Process. 41 (2016) 45–53.
[5] S. Francoeur, M.J. Seong, A. Mascarenhas, S. Tixier, M. Adamcyk, T. Tiedje, Appl. Phys. Lett. 82 (2003) 3874.
[6] B. Fluegel, S. Francoeur, A. Mascarenhas, S. Tixier, E.C. Young, T. Tiedje, Phys. Rev. Lett. 97 (2006) 067205.
[7] R.B. Lewis, D.A. Beaton, X. Lu, T. Tiedje, J. Crystal Growth 311 (2009) 1872.
[8] J. Yoshida, T. Kita, O. Wada, K. Oe, Jpn. J. Appl. Phys. 42 (2003) 371.
[9] W. Huang, K. Oe, G. Feng, M. Yoshimoto, J. Appl. Phys. 98 (2005) 053505.
[10] S.K. Das, T.D. Das, S. Dhar, M. de la Mare, A. Krier, Infrared Phys. Technol. 55 (2012) 156–160.
[11] A. Janotti, Su-Huai Wei, S.B. Zhang, Phys. Rev. B 65 (2002) 115203.
[12] K. Alberi, J. Wu, W. Walukiewicz, K.M. Yu, O.D. Dubon, S.P. Watkins, C.X. Wang, X. Liu, Y.-J. Cho, J. Furdyna, Phys. Rev. B 75 (2007) 045203.
[13] V. Virkkala, V. Havu, F. Tuomisto, M.J. Puska, Phys. Rev. B 88 (2013) 035204.
[14] V. Virkkala, V. Havu, F. Tuomisto, M.J. Puska, Phys. Rev. B 85 (2012) 085134.
[15] G. Pettinari, A. Polimeni, M. Capizzi, J.H. Blokland, M. Christianen, J.C. Maan, E. C. Young, T. Tiedje, Appl. Phys. Lett. 92 (2008) 262105.
[16] A. Lindsay, E.P. O'Reilly, A.D. Andreev, T. Ashley, Phys. Rev. B 77 (2008) 165205.
[17] A. Mascarenhas, Yong Zhang, Curr. Opin. Solid State Mater. Sci. 5 (2001) 253–259.

[18] R.N. Kini, L. Bhusal, A.J. Ptak, R. France, A. Mascarenhas, J. Appl. Phys. 106 (2009) 043705.
[19] K. Oe, Jpn. J. Appl. Phys. 41 (2002) 2801–2806.
[20] E.C. Young, M.B. Whitwick, T. Tiedje, D.A. Beaton, Phys. Status Solidi 4 (2007) 1707–1710.
[21] K. Wang, Y. Gu, H.F. Zhou, L.Y. Zhang, C.Z. Kang, M.J. Wu, W.W. Pan, P.F. Lu, Q. Gong, S.M. Wang, Sci. Rep. 4 (2014) 5449.
[22] S.C. Das, T.D. Das, S. Dhar, Infrared Phys. Technol. 55 (2012) 306–308.
[23] M.K. Rajpalke, W.M. Linhart, K.M. Yu, T.S. Jones, M.J. Ashwin, T.D. Veal, J. Cryst. Growth 425 (2015) 241–244.
[24] I. Vurgaftman, J.R. Meyer, L.R. Ram-Mohan, J. Appl. Phys. 89 (2001) 5815–5875.
[25] N.A.A. Rahim, R. Ahmed, B. Ul Haq, M. Mohamad, A. Shaari, N. Ali, S. Goumri-Said, Comput. Mater. Sci 114 (2016) 40–46.
[26] Mid-infrared Semiconductor Optoelectronics, in: A. Krier (Ed.), Springer Verlag London Limited, 2006.
[27] S.A. Barnett, J. Vac. Sci. Technol. 5 (1987) 2845.
[28] K.Y. Ma, Z.M. Fang, D.H. Jaw, R.M. Cohen, G.B. Stringfellow, W.P. Kosar, D.W. Brown, Appl. Phys. Lett. 55 (1989) 2420.
[29] Z.M. Fang, K.Y. Ma, R.M. Cohen, G.B. Stringfellow, J. Appl. Phys. 68 (1990) 1187.
[30] H. Okamoto, K. Oe, Jpn. J. Appl. Phys. 37 (1998) 1608–1613.
[31] S.P. Svensson, H. Hier, W.L. Sarney, D. Donetsky, D. Wang, G. Belenky, J. Vac. Sci. Technol. 30 (2012) 109.
[32] I.C. Sandall, F. Bastiman, B. White, R. Richards, D. Mendes, J.P.R. David, C.H. Tan, Appl. Phys. Lett. 104 (2014) 171109.
[33] J. Lu, P.T. Webster, S. Liu, Y.-H. Zhang, S.R. Johnson, D.J. Smith, J. Cryst. Growth 425 (2015) 250–254.
[34] M.P. Polak, P. Scharoch, R. Kudrawiec, Semicond. Sci. Technol. 30 (2015) 094001.
[35] D.P. Samajdar, T.D. Das, S. Dhar, Comput. Mater. Sci 111 (2016) 497–502.
[36] D.P. Samajdar, S. Dhar, Physica B 484 (2016) 27–30.
[37] A.G. Milnes, A.Y. Polyakov, Mater. Sci. Eng. B (1993) 18–237.
[38] D.H. Chow, H.L. Dunlap, W. Williamson, S. Enquist, B.K. Gilbert, S. Subramaniam, P.-M. Lei, G.H. Bernstein, IEEE Electron Device Lett. (1996) 17–69.
[39] J.W.J. Slavin, D. Zemlyanov, A. Ivanisevic, Surf. Sci. (2009) 603–690.
[40] K.H. Hellwege, O. Madelung, Landolt-Bornstein, Semiconductors Physics of Group IV Elements and III–V Alloys, New Series, Group III, (1982) .
[41] P. Hohenberg, W. Kohn, Phys. Rev. B 136 (1964) 864.
[42] W. Kohn, L.J. Sham, Phys. Rev. A 140 (1965) 1133.
[43] P. Blaha, K. Schwarz, G.K.H. Madsen, D. Kvasnicka, J. Luitz, WIEN2k An Augmented Plane Wave + Local Orbitals Program for Calculating Crystal Properties, Karlheinz Schwarz, Techn. Universität Wien, Austria, 2001 (ISBN: 3-9501031-1-2).
[44] Z. Wu, R.E. Cohen, Phys. Rev. B 73 (2006) 235116.
[45] P. Blaha Tran, Phys. Rev. Lett. 102 (2009) 226401.
[46] W.G. Aulbur, L. Jönsson, J.W. Wilkins, Solid State Phys. 54 (2000) 1.
[47] S. Zh Karazhanov, P. Ravindran, H. Fjellvag, B.G. Svensson, J. Appl. Phys. 106 (2009) 123701.
[48] D. Allali, A. Bouhemadou, E. Muhammad AbudAlSafi, S. Bin-Omran, M. Chegaar, R. Khenata, A.H. Reshak, Physica B 443 (2014) 24–34.
[49] David Koller, Fabien Tran, Peter Blaha, Phys. Rev. B 85 (2012) 155109.
[50] H.J. Monkhorst, J.D. Pack, Phys. Rev. 13 (1976) 5188.
[51] F.D. Murnaghan, Proc. Natl. Aced. Sci. U. S. A 30 (1944) 244–247.
[52] S. Adachi, Properties of Semiconductor Alloys: Group-IV, III?V and II?VI Semiconductors, JohnWiley & Sons, Ltd., Chichester, 2009.
[53] M. Hadjab, S. Berrah, H. Abid, M.I. Ziane, H. Bennacer, B.G. Yalcin, Optik 127 (2016) 9280–9294.
[54] M. Briki, M. Abdelouhab, A. Zaoui, M. Ferhat, Superlattices Microstruct. 45 (2009) 80–90.
[55] M. Aslan, B.G. Yalcin, M. Ustundag, J. Alloy. Compd. 519 (2012) 55–59.
[56] S. Massidda, A. Continenza, A.J. Freeman, T.M. de Pascale, F. Meloni, M. Serra, Phys. Rev. B 41 (17) (1990) 12078–12085.
[57] L. Vegard, Z. Phys. 5 (1921) 17–26.
[58] K.Y. Ma, Z.M. Fang, R.M. Cohen, G.B. Stringfellow, J. Cryst. Growth 107 (1991) 416–421.
[59] K.T. Huang, C.T. Chiu, R.M. Cohen, G.B. Stringfellow, J. Cryst. Growth 134 (1993) 29–34.
[60] M.K. Rajpalke, W.M. Linhart, K.M. Yu, M. Birkett, J. Alaria, J.J. Bomphrey, S. Sallis, L.F.J. Piper, T.S. Jones, M.J. Ashwin, T.D. Veal, Appl. Phys. Lett. 105 (2014) 212101.
[61] A. Assali, M. Bouslama, A.H. Reshak, Samir Zerroug, H. Abid, Optik 135 (2017) 57–69.
[62] A.H. Reshak, Z. Charifi, H. Baaziz, Sol. Energy 90 (2013) 134–143.
[63] N. Souza Dantas, J.S. de Almeida, R. Ahuja, C. Persson, A. Ferreira da Silva, Appl. Phys. Lett. 92 (2008) 121914.
[64] A. Assali, M. Bouslama, Infrared Phys. Technol. 81 (2017) 175–181.
[65] M.J. Winiarski, Comput. Mater. Sci 108 (2015) 14–16.
[66] A. Assali, M. Bouslama, H. Abid, S. Zerroug, M. Ghaffour, F. Saidi, L. Bouzaiene, K. Boulenouar, Mater. Sci. Semicond. Process. 36 (2015) 192–203.
[67] S. Adachi, Properties of Group-IV, III–V and II–VI Semiconductors, John Wiley & Sons, England, 2005.
[68] M.P. Thompson, G.W. Auner, T.S. Zheleva, K.A. Jones, S.J. Simko, J.N. Hilfiker, J. Appl. Phys. 89 (2001) 3321.
[69] M.I. Ziane, Z. Bensaad, B. Labdelli, H. Bennacer, Sensors Transducers 27 (2014) 374–384.
[70] R. Ahmed, S.J. Hashemifar, H. Akbarzadeh, M. Ahmed, F. e-Aleem, Comput. Mater. Sci 39 (2007) 580–586.
[71] S. Zh Karazhanov, L.C. Lew, Y. Voon, Semiconductors 39 (2005) 161–173.
[72] M.D. McCluskey, C.G. Van de Walle, C.P. Master, L.T. Romano, N.M. Johnson, Appl. Phys. Lett. 72 (1998) 2725.
[73] A. Ben Fredj, M. Debbichi, M. Said, Microelectron. J. 38 (2007) 860–870.
[74] L. Bellaiche, T. Mattila, L.W. Wang, S.H. Wei, A. Zunger, Appl. Phys. Lett. 74 (1999) 1842.
[75] M. Rabah, B. Sahraoui, B. Bouhafs, B. Abbar, H. Abid, Phys. Stat. Sol. 238 (2003) 156.
[76] M.G. Moreno-Arnenta, L. Mancera, N. Takeuchi, Phys. Stat. Sol. 238 (2003) 127.
[77] G.P. Srivastava, J.L. Martins, A. Zunger, Phys. Rev. B 31 (1985) 2561.
[78] H. Okamoto, K. Oe, Jpn. J. Appl. Phys. 38 (1999) 1022–1025.
[79] S. Adachi, Optical Properties of Crystalline and Amorphous Semiconductors: Materials and Fundamental Principles, Kluwer Academic Publishers, Boston, 1999.
[80] C.A. Draxl, R. Abt, ICTP Lecture Notes, (1998) (unpublished).
[81] P.Y. Yu, M. Cardona, Fundamentals of Semiconductors: Physics and Materials Properties, Springer-Verlag, Berlin, 1999, pp. 233.
[82] Y. Zhang, W.M. Shen, Basic of Solid Electronics, Zhejiang University Press, Hangzhou, 2005.
[83] V. Antonov, B. Harmon, A. Yaresko, Electronic Structure and Magneto-Optical Properties of Solids, Kluwer Academic Publishers, New York, 2004.
[84] M. Cardona, J. Phys. Chem. Solids 24 (1963) 1543.
[85] D.E. Aspnes, A.A. Studna, Appl. Phys. Lett. 39 (1981) 316.
[86] S.H. Rhim, Miyoung Kim, A.J. Freeman, Phys. Rev. B 71 (2005) 045202.
[87] Tae Jung Kim, Jae Jin Yoon, Soon Yong Hwang, Yong Woo Jung, T. Ghong, Tae Ho Kim, Young Dong Kim, Yia-Chung Chang, Appl. Phys. Lett. 97 (2010) 171912.
[88] S. Adachi, J. Appl. Phys. 66 (1989) 6030.
[89] N.M. Ravindra, V.K. Srivastava, Infrared Phys. 19 (1979) 603.
[90] M. Hass, B.W. Henvis, J. Phys. Chem. Solids 23 (1962) 1099.
[91] B.R. Bennet, R.A. Soref, Senior Member, IEEE J. Quantum Electron. 23 (1987) 12.
[92] D.E. Aspnes, A.A. Studna, Phys. Rev. B 27 (1983) 985–1009.
[93] H.R. Philipp, H. Ehrenreich, Phys. Rev. 129 (1963) 1550.
[94] M. Yousaf, M.A. Saeed, R. Ahmed, M.M. Alsardia, A. Mat Isa, A. Shaari, Commun. Theor. Phys. 58 (2012) 777–784.
[95] Ali. Hussain Reshak, H. Kamarudin, S. Auluck, J. Alloys Compd. 509 (2011) 9685–9691.